



PEDOT-functionalized carbon nanotubes for anticorrosive reinforcement of epoxy coatings on sintered NdFeB magnets

Zihan Shen, Hongyi Yang, Pengjie Zhang, Jiewu Cui, Dongmei Wang, Wangqiang Shen, Guangqing Xu , Jun Lv

Received: 5 October 2023 / Revised: 4 February 2024 / Accepted: 6 February 2024
© American Coatings Association 2024

Abstract Solving the problems of interfacial compatibility and dispersibility between filler and epoxy resin (EP) can greatly improve the anticorrosion performances of epoxy coatings and expand their application field. In this work, carbon nanotubes (CNTs) were modified by poly(sodium 4-styrene sulfonate) and poly(3,4-ethylenedioxythiophene) to form PCNTs hybrids, and the cathodic electrophoretic deposition method was used to form composite epoxy coatings on the surface of sintered NdFeB magnets for enhancing the anticorrosion performance. The corrosion resistance of PCNTs was evaluated by electrochemical and static immersion corrosion tests. Results indicate that PCNTs hybrids possess better distribution and compatibility in epoxy resin than CNTs hybrids, resulting in the anticorrosion performances of higher density of composite epoxy coatings on NdFeB magnets. Optimized EP/PCNTs possess a much higher $|Z|_{0.01 \text{ Hz}}$ of $4.41 \times 10^7 \Omega\text{-cm}^2$ and a much lower J_{corr} of

$9.648 \times 10^{-10} \text{ A}\cdot\text{cm}^{-2}$ than that of EP ($1.34 \times 10^4 \Omega\text{-cm}^2$ and $J_{\text{corr}} 4.436 \times 10^{-6} \text{ A}\cdot\text{cm}^{-2}$), demonstrating superior corrosion resistance.

Keywords NdFeB magnets, Epoxy coatings, PEDOT-modified CNTs, Corrosion resistance

Introduction

Sintered NdFeB magnets are widely used in various industrial fields due to their excellent magnetic properties.¹ They have occupied a core position in the permanent magnets market and are used in 5G communications, high-end medical equipment, wind power generation, and electric vehicles. However, the multiphase structure of NdFeB magnets results in poor corrosion resistance, which can affect the stability and safety of the magnets during service.²

There are two main methods for improving the corrosion resistance of NdFeB magnets: the addition of alloying elements^{3–5} and surface protective coatings. The microstructure of the Nd-rich phases can be improved and the density of the magnet can be increased by adding alloying elements, which reduces the potential difference among different phases of the magnets.⁶ While the addition of alloy elements can enhance the corrosion resistance of magnets to some extent, the effect is limited. In some cases, the nonmagnetic alloying phases can lead to a decrease in magnetic properties.⁷

By applying a protective coating to the surface of sintered NdFeB magnets, they can be shielded from external corrosive mediums, thus delaying their corrosion. Various coatings have been studied and applied to NdFeB magnets, including metal coatings,^{8,9} organic coatings,¹⁰ and ceramic coatings.^{11,12} Commonly used metal coatings, such as Zn, Ni, and Al,¹³ are prepared using electroless plating, electroplating, and physical

Z. Shen, H. Yang, J. Cui, D. Wang, W. Shen, G. Xu (✉),
J. Lv (✉)
School of Materials Science and Engineering, Hefei
University of Technology, Hefei 230009, China
e-mail: gqxu1979@hfut.edu.cn

J. Lv
e-mail: lvjun@hfut.edu.cn

P. Zhang
BGRIMM Magnetic Materials and Technology Co., Ltd,
Beijing 102600, China

J. Cui, D. Wang, W. Shen, G. Xu, J. Lv
Key Laboratory of Advanced Functional Materials and
Devices of Anhui Province; Anhui Provincial International
S&T Cooperation Base for Advanced Energy Materials,
Engineering Research Center of High-Performance Copper
Alloy Materials and Processing, Ministry of Education,
Hefei University of Technology, Hefei 230009, China

vapor deposition methods. The ceramic coatings used to protect NdFeB are primarily Al_2O_3 and SiO_2 . These coatings can be prepared using physical vapor deposition, microarc oxidation, and other methods. In a study by Ding et al.,¹⁴ Cr_2O_3 coatings were prepared on NdFeB magnets using ion beam-assisted pulsed magnetron sputtering. This process not only improved the magnets' corrosion resistance but also enhanced their mechanical properties. In recent years, research and development of organic coating protection systems on the surface of NdFeB magnets has been limited to silane and epoxy resin coatings. Hu et al.¹⁵ investigated the effect of silane treatment on the corrosion resistance of NdFeB magnets. They found that the corrosion resistance of magnets could be significantly improved by silane treatment after phosphate or chromate passivation. Xu et al.¹⁶ deposited epoxy resin/ TiO_2 composite coatings on NdFeB magnets using electrophoresis. The addition of TiO_2 reduces the edge and corner effect of the coating, providing better protection for the corners of the magnets.

Epoxy resins are thermosetting resins that cure using a variety of curing agents through curing reactions. They are easy to prepare and contain fewer volatile organic compounds. Epoxy coatings are widely used due to their excellent mechanical properties, strong adhesion, electrical insulation, good heat resistance, and chemical stability.¹⁷ However, the long-term application of epoxy coatings to protect sintered NdFeB magnets is seriously limited due to defects inside the coating caused by the volatilization of water during the solidification process.¹⁸ To enhance the anticorrosion performance of epoxy coatings, one effective approach is to incorporate fillers into the coating to decrease defects. These fillers can include graphene,¹⁹ metal organic framework,²⁰ h-BN,^{21,22} ZnO ,^{23,24} CeO_2 ,²⁵ and carbon nanotubes (CNTs).^{26,27} CNTs have attracted attention due to their high chemical and thermal stability, making them stable in corrosive medium.

However, the application of epoxy coatings based on carbon nanotubes is often hindered by the incompatibility of carbon nanotubes with epoxy resin systems and the uneven dispersion caused by carbon nanotube agglomeration. In recent years, there has been a growing interest in conductive polymer-based organic/inorganic composites as fillers to improve the dispersion and compatibility of nanomaterials in epoxy coatings.^{21,28,29} These composites, when combined with inorganic nanomaterials, have a synergistic effect that can significantly enhance the anticorrosive performance of epoxy coatings. Najmi et al.²⁷ incorporated Zn-doped polyaniline functionalized CNTs into epoxy coatings, resulting in excellent barrier self-healing corrosion protection. The active inhibition of Zn-doped polyaniline and the improved compatibility and homogeneousness of CNTs in the polymer matrix, due to polyaniline grafting, contributed to the enhanced performance. Nayak et al.³⁰ prepared a composite of f-CNTs/polyindole as a pigment, which

exhibited excellent dispersibility in the epoxy matrix. This composite showed a significant enhancement in barrier protection and anticorrosion performance of epoxy coatings. Cui and colleagues³¹ reported the preparation of modified epoxy coatings with CNTs/poly(2-butyl aniline) as reinforcement. Modifying CNTs with poly(2-butylaniline) can improve the dispersion and compatibility of CNTs in the epoxy matrix, thereby enhancing the shielding effect of CNTs/epoxy composite coatings.

Poly(3,4-ethylenedioxythiophene) (PEDOT) is a conductive polymer with several advantages, including easy synthesis, nontoxicity, excellent compatibility, environmental stability, and satisfactory stretchability. These properties make it a promising candidate for use in the field of corrosion protection.^{32–34} However, there is still insufficient research on the use of PEDOT and its composites as reinforcement for epoxy anticorrosive coatings.^{35–38}

The study aimed to improve the homogeneity and compatibility of carbon nanotubes (CNTs) in waterborne epoxy coatings by modifying them with poly(sodium 4-styrene sulfonate) (PSS) and PEDOT, forming PCNTs hybrids. The results showed that the PCNTs hybrids can enhance the anticorrosion performance of epoxy resin coatings on NdFeB magnets.

Experimental

Materials

Commercial sintered NdFeB magnets (unmagnetized 38SH, 12 mm × 13 mm × 3 mm) were purchased from Earth-panda Advanced Magnetic Material Co., Ltd. Carboxylated CNTs with carboxyl content of around 0.73 wt% were supplied by Nanjing Xianfeng Nano Materials Co., Ltd. Poly(sodium 4-styrenesulfonate) (PSS, average Mw ~ 70000, 30 wt% in H_2O), 3,4-ethylenedioxythiophene (EDOT) and sodium persulfate ($\text{Na}_2\text{S}_2\text{O}_8$, AR) were purchased from Aladdin Chemical Co., Ltd. (Shanghai). Nitric acid (AR) and absolute ethyl alcohol (AR) were supplied by Sino-pharm Chemical Reagent Co., Ltd. Waterborne epoxy resin (EP, HG-90 series, particle size $\leq 20 \mu\text{m}$, solid content of $36 \pm 2\%$, pH of 7.0 ± 0.3 , conductivity of $1100 \pm 300 \mu\text{s}/\text{cm}$) and black slurry (48–52% distilled water, 8–12% 2-butoxyethanol, 5% carbon black, 15% kaolin, 18–22% water-soluble solid) used for coloring were supplied by Brilliant Electrophoresis Co., Ltd. (Shenzhen, China). Deionized water with a resistance of $18.2 \text{ M}\Omega\cdot\text{cm}$ was produced by a water purification device.

Synthesis of PCNTs hybrids

PCNTs hybrids were obtained by modifying CNTs with PEDOT synthesized by polymerization of EDOT in

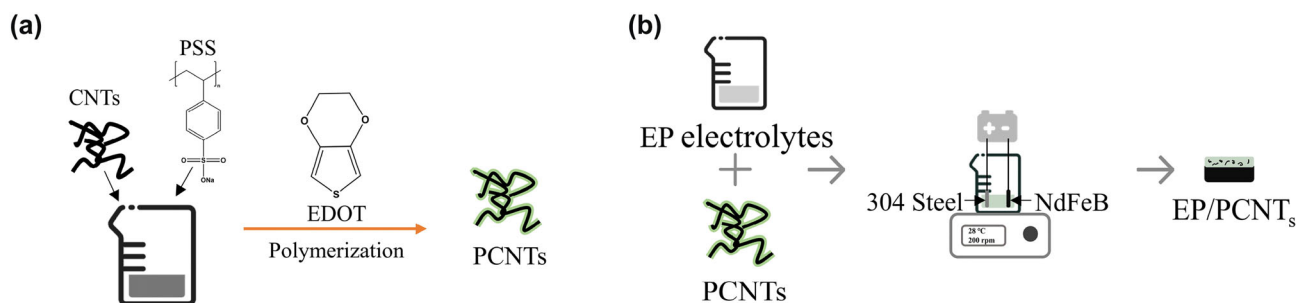


Fig. 1: Schematic diagrams of PCNTs hybrids synthesis (a) and electrophoretic deposition of PCNTs hybrids on the surface of NdFeB magnets (b)

the presence of PSS. The synthesis process of PCNT hybrids is shown in Fig. 1a. First, 0.53 g of PSS was dissolved in 100 mL of distilled water with vigorous stirring. Then, 100 mg of carboxylated CNTs was added to the mixture and sonicated for 1 h. Later, 0.8 mL of EDOT monomer was added to the solution and fully dispersed. Subsequently, 0.96 g of $\text{Na}_2\text{S}_2\text{O}_8$ was added to the mixture to initiate the polymerization reaction. The reaction was carried out at 30°C for 24 h. Finally, the PCNTs hybrids were collected by vacuum drying at 60°C for 24 h after being centrifuged and washed several times with a water–ethanol solvent ($v/v = 2:3$).

Electrophoretic deposition of epoxy coatings

Composite epoxy coatings were prepared using a cathodic electrophoretic deposition process in an aqueous solution containing deionized water, waterborne epoxy resin, and black slurry aqueous suspension in a mass ratio of 4:3:1, as shown in Fig. 1b. To enhance the coatings, PCNT hybrids with varying contents of 2, 4, 6, and 8 g/L were added to the aqueous suspension. For comparison purposes, 2 g/L of unmodified CNTs was also included in the suspension for subsequent electrophoretic deposition.

Electrophoretic deposition was performed using a constant voltage method. A NdFeB magnet was used as the working electrode, while 304 stainless steel was used as the counter electrode. The temperature was maintained at 28°C. All specimens were deposited at 60 V for 45 s. They were then cured for 40 min at 90°C, followed by an additional 30 min at 180°C. The obtained specimens were designated as EP and EP/CNTs₂, referring to pure epoxy resin specimens and specimens modified with pristine CNTs (2 g/L). The specimens containing PCNT hybrids were designated as EP/PCNTs₂, EP/PCNTs₄, EP/PCNTs₆, and EP/PCNTs₈, respectively.

Material characterizations and corrosion resistance tests

The compositions and structures of the modified carbon nanotubes (CNTs) were analyzed using Fourier transform infrared (FTIR) spectra on a Nicolet 6700 spectrometer (Thermo Nicolet, US), Raman spectroscopy on a LabRam HR Evolution (HORIBA Jobin Yvon, FR) with a wavelength of 532 nm from 800 to 2000 cm^{-1} , and X-ray diffraction (XRD) on an X-Pert Pro MPD (PANalytical, NL) with Cu K α radiation from 5° to 80°, respectively. The X-ray photoelectron spectroscopy (XPS) analysis on an ESCLAB 250Xi (Thermo, US) with Al K α X-ray source detected the surface chemical states of the PCNTs. The morphologies of composited coatings on NdFeB magnets were observed using a field emission scanning electron microscope (FESEM, Hitachi SU8020, JP).

The corrosion behaviors of the specimens were investigated through electrochemical measurement and static full immersion corrosion test. The electrochemical measurement was conducted using a three-electrode system on a Chenhua CHI-660D electrochemical workstation. The working electrode was EP/PCNTs specimens with an exposed area of 1 cm^2 , while a saturated calomel electrode (SCE) served as the reference electrode and a platinum sheet as the counter electrode. Prior to the test, all specimens were immersed in a 3.5 wt% NaCl solution for 30 min to obtain a stable potential. Impedance spectroscopy (EIS) was performed in open-circuit potential (OCP) mode using an AC amplitude of 20 mV over a frequency range of 10^{-2} – 10^5 Hz. Potentiodynamic polarization curves were collected at a scan rate of 0.01 V/s from –0.3 V to 0.3 V (vs. OCP). The surface changes of the specimens soaked in a 3.5 wt% NaCl solution for a certain time were observed through static immersion corrosion testing.

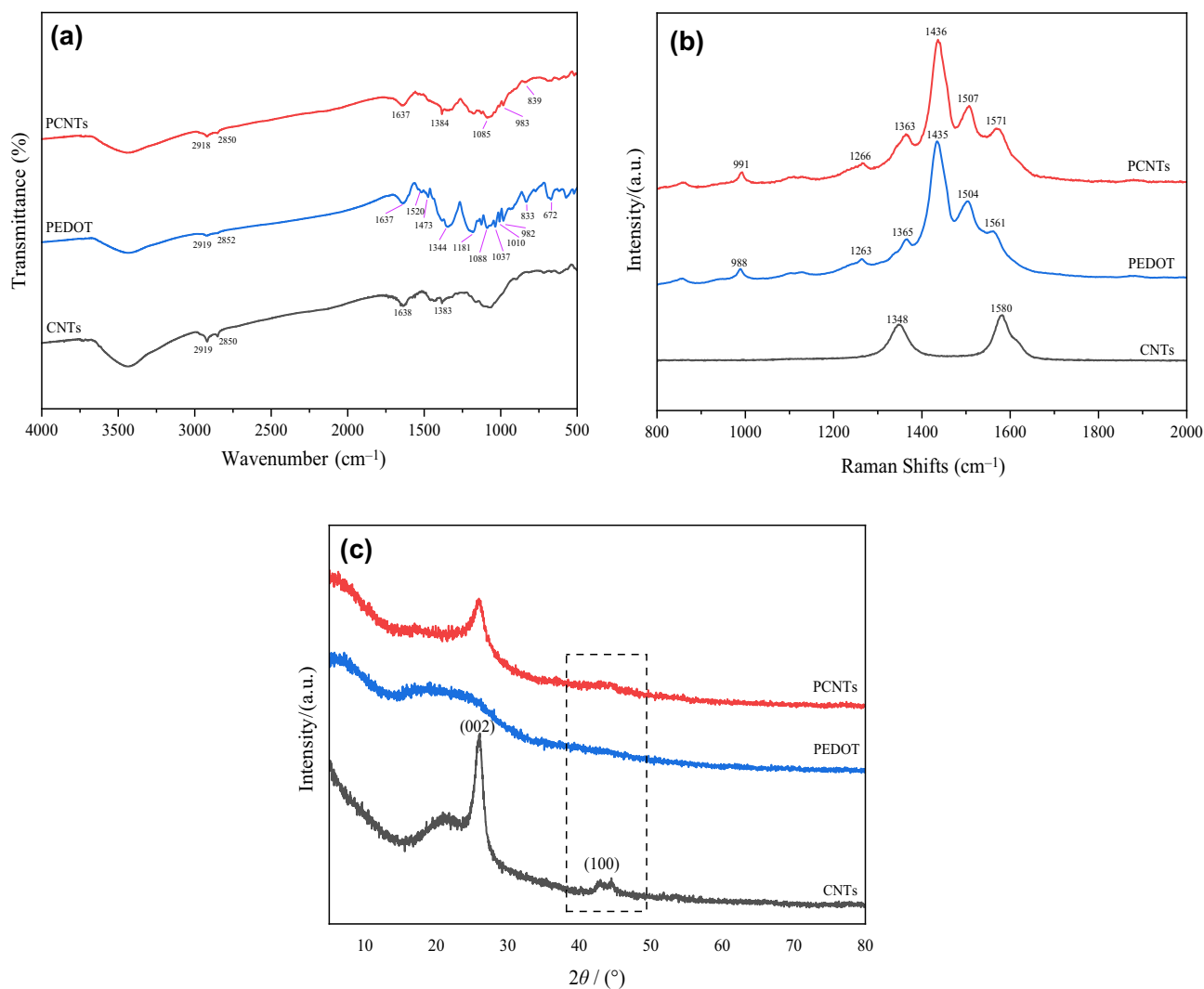


Fig. 2: FTIR spectra (a), Raman spectra (b), and XRD patterns (c) of CNTs, PEDOT, and PCNTs

Results and discussion

Characterization of PCNTs hybrids

FTIR, Raman, and XRD were used to investigate the composition and structure of the filler, as shown in Fig. 2. Figure 2a displays the FTIR patterns of CNTs, PEDOT, and PCNTs. CNTs exhibit vibrational peaks at 2919, 2850, and 1638 cm⁻¹, which correlate with -CH₃, -CH₂, and C=C groups,^{39,40} respectively. The FTIR pattern of PEDOT reveals a typical band at around 1520 cm⁻¹, which is attributed to the asymmetric stretching vibrations of the quinoid structure of PEDOT. A lower frequency and intensity of this band indicate a more reduced PEDOT. The strongest and broadest band at 1344 cm⁻¹ is due to a superposition of the C=C symmetric, C-C ring, and inter-ring C-C stretching vibrations of the thiophene rings.^{41–43} Addi-

tionally, peaks at 982, 833, and 672 cm⁻¹ are derived from the vibration of the C-S bond of the thiophene ring.^{44,45} Additionally, peaks at 1181, 1037, and 1010 cm⁻¹ are indexed to the -SO₃ group in PSS.^{46,47} In the curve of PCNTs hybrids, the infrared characteristic peaks of CNTs and PEDOT can be observed, indicating the successful polymerization of PEDOT on CNTs.

The Raman spectra of CNTs, PEDOT, and PCNTs are shown in Fig. 2b, where the D band and G band are observed at 1348 and 1580 cm⁻¹, respectively, for CNTs. The Raman spectrum of PEDOT shows peaks at 988, 1263, and 1365 cm⁻¹, which correspond to the oxyethylene ring deformation, C_x-C_x inter-ring stretching, and single C_β-C_β stretching, respectively.⁴⁸ The peak at 1435 cm⁻¹ corresponds to the symmetrical vibration of C_α = C_β, while the antisymmetric stretching mode of C_α = C_β, which corresponds to the

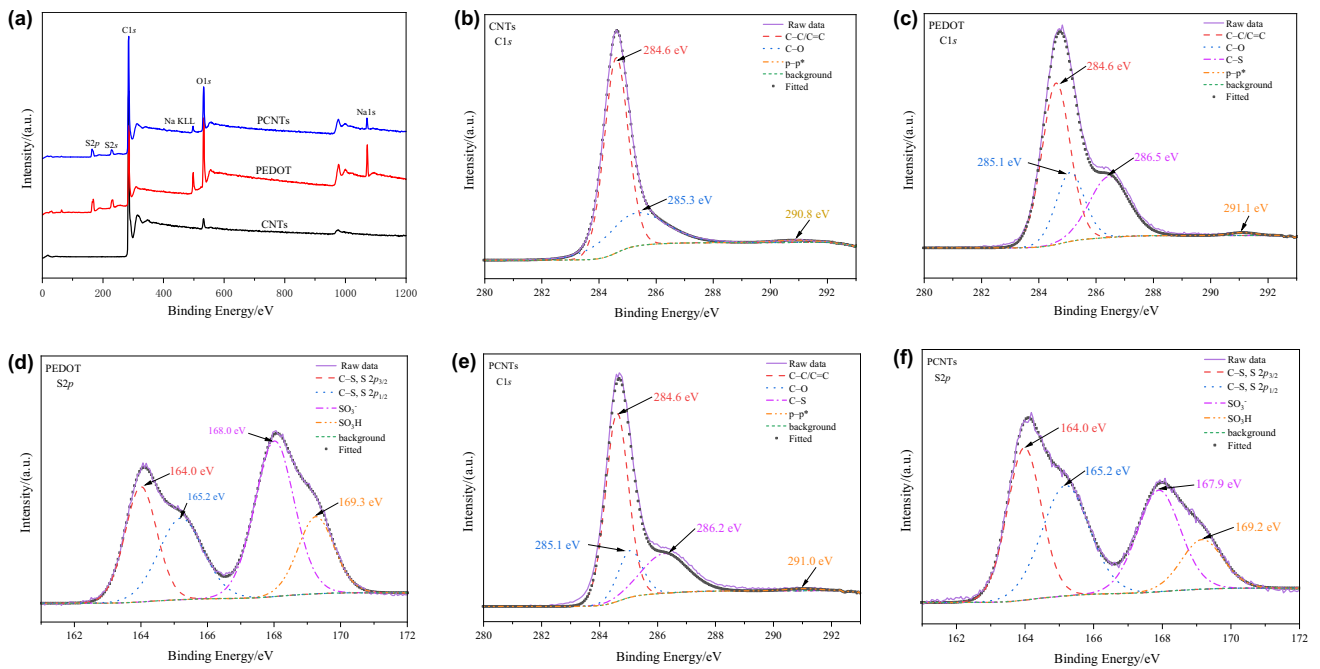


Fig. 3: XPS spectra of CNTs, PCNTs, and PEDOT: (a) survey patterns, (b) high resolution patterns of C1s electrons in CNTs, (c) C1s electrons in PEDOT, (d) S2p electrons in PEDOT, (e) C1s electrons in PCNTs, (f) S2p electrons in PCNTs

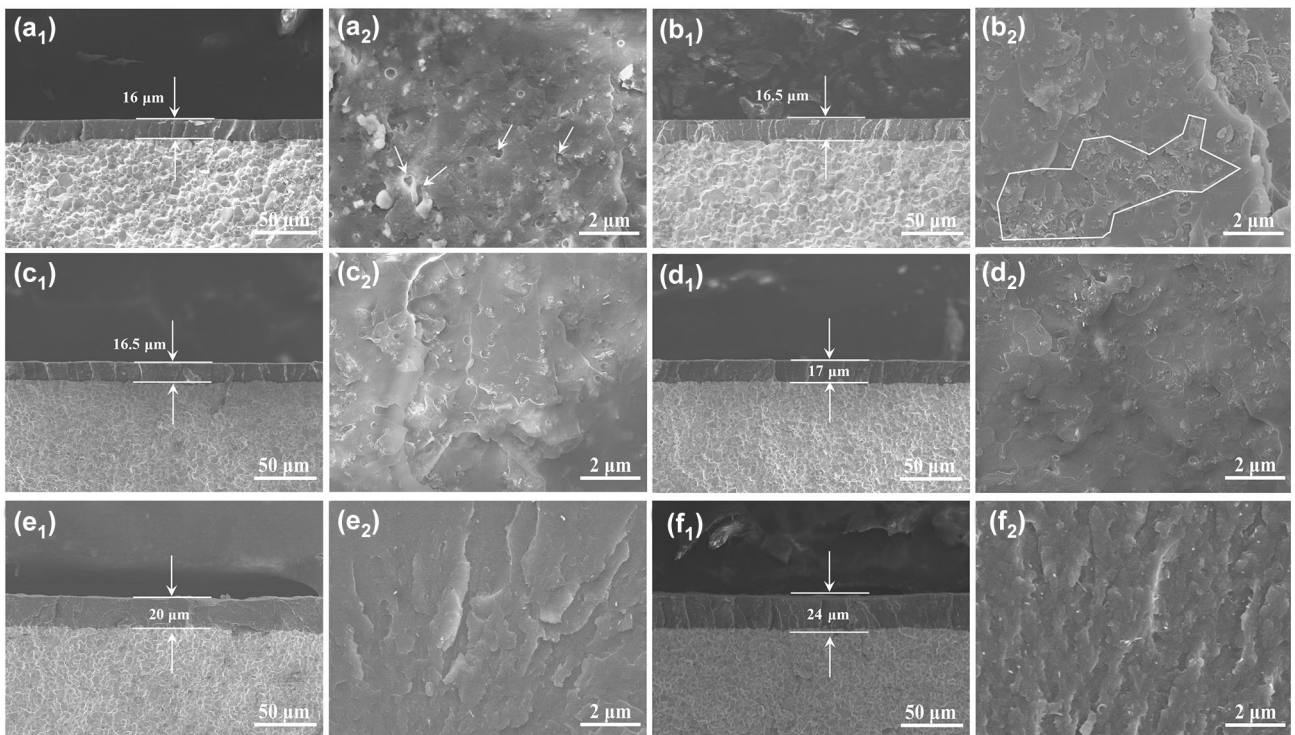
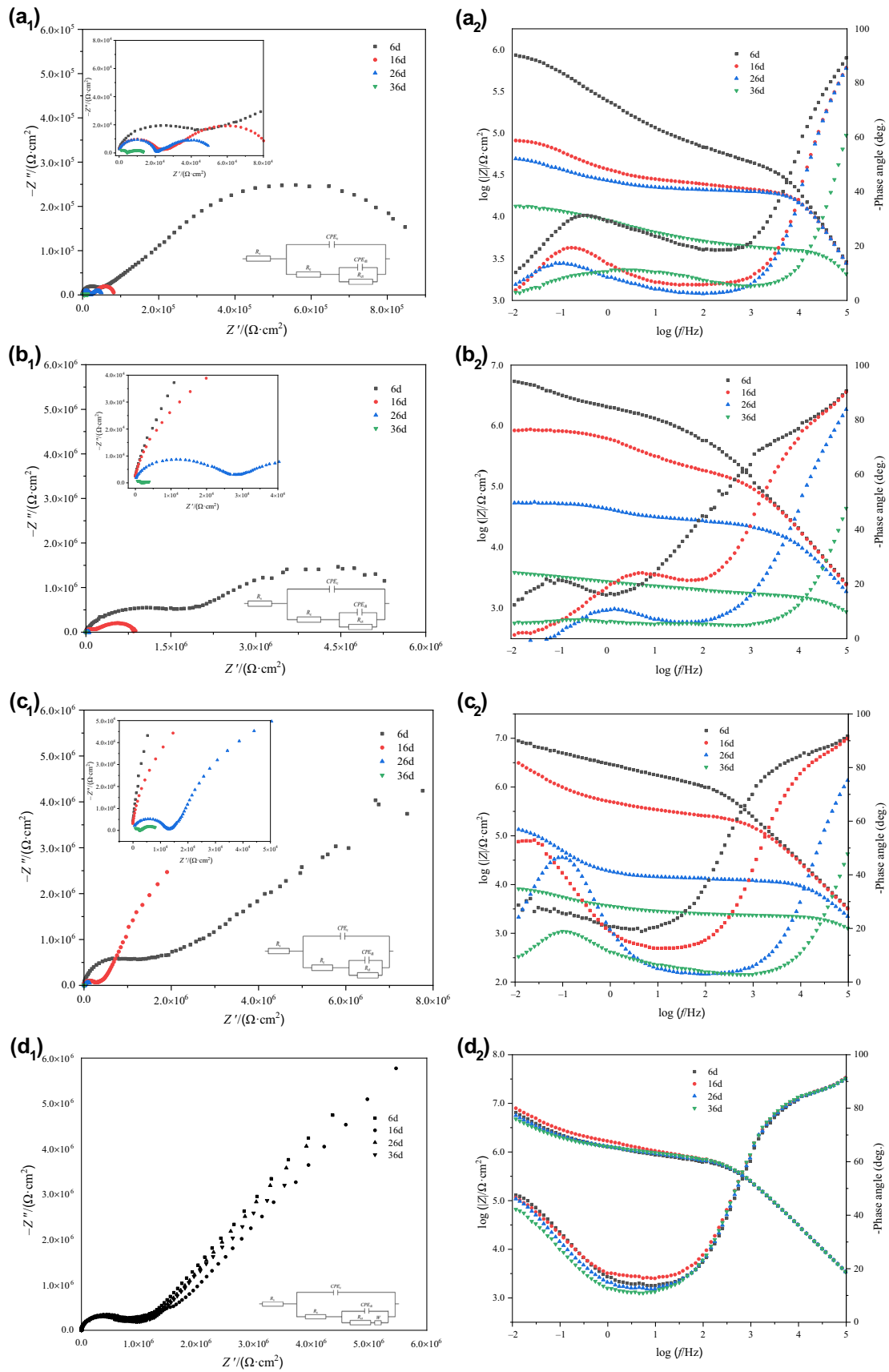


Fig. 4: Cross-sectional and surface SEM morphologies of EP (a), EP/CNTs₂ (b), EP/PCNTs₂ (c), EP/PCNTs₄ (d), EP/PCNTs₆ (e) and EP/PCNTs₈ (f)



◀ **Fig. 5: Nyquist and Bode plots of different specimens after being immersed in 3.5 wt% NaCl solution for different times: (a) EP, (b) EP/CNTs₂, (c) EP/PCNTs₂, (d) EP/PCNTs₄, (e) EP/PCNTs₆, (f) EP/PCNTs₈**

thiophene rings in the middle and at the end of the polymer chain, appears at 1504 and 1561 cm⁻¹.^{48,49} It is worth noting that the peaks of PCNTs are slightly shifted compared to those of PEDOT. Specifically, the peaks of the oxyethylene ring deformation, C_α-C_α inter-ring stretching, and single C_β-C_β stretching move to 991, 1266, and 1363 cm⁻¹, respectively. This confirms the presence of strong interfacial interactions between PEDOT and CNTs, including π-π interaction and van der Waals forces.³⁹

Figure 2c shows the XRD patterns of CNTs, PEDOT, and PCNTs. The XRD spectrum of CNTs shows peaks at 26.0° and 42.9°, which are assigned to (002) and (100) crystal planes of a graphite-like structure.^{27,50} In contrast, PEDOT does not exhibit any characteristic diffraction peak in its XRD spec-

trum, indicating its amorphous structure. However, after modification with PEDOT, the characteristic diffraction peaks of the (002) and (100) crystal planes are still present with lower intensity due to the sheltering effect of PEDOT.

The surface chemical states of the CNTs, PEDOT, and PCNTs were analyzed using XPS, as illustrated in Fig. 3. The survey patterns in Fig. 3a indicate that, in addition to carbon and oxygen, PEDOT and PCNTs contain mainly sulfury and sodium elements. The sodium is derived from the residues of PSS or Na₂S₂O₈ in the synthesis process. The C1s spectra of CNTs (Fig. 3b) show three peaks centered at 284.6, 285.3, and 290.8 eV, corresponding to C-C/C=C, C-O, and π-π* bonds, respectively.⁵¹⁻⁵³ The C1s spectra of PEDOT (Fig. 3c) show a new peak at 286.5 eV corresponding to C-S from thiophene rings. The S2p spectra of PEDOT show four peaks centered around 164.0, 165.2, 168.0, and 169.3 eV, ascribing to C-S of PEDOT and -SO₃ group of PSS.^{54,55} The presence of PSS and PEDOT peaks in PCNTs confirms the successful modification of CNTs with PEDOT and PSS, which is further supported by the FTIR analysis in Fig. 2a.

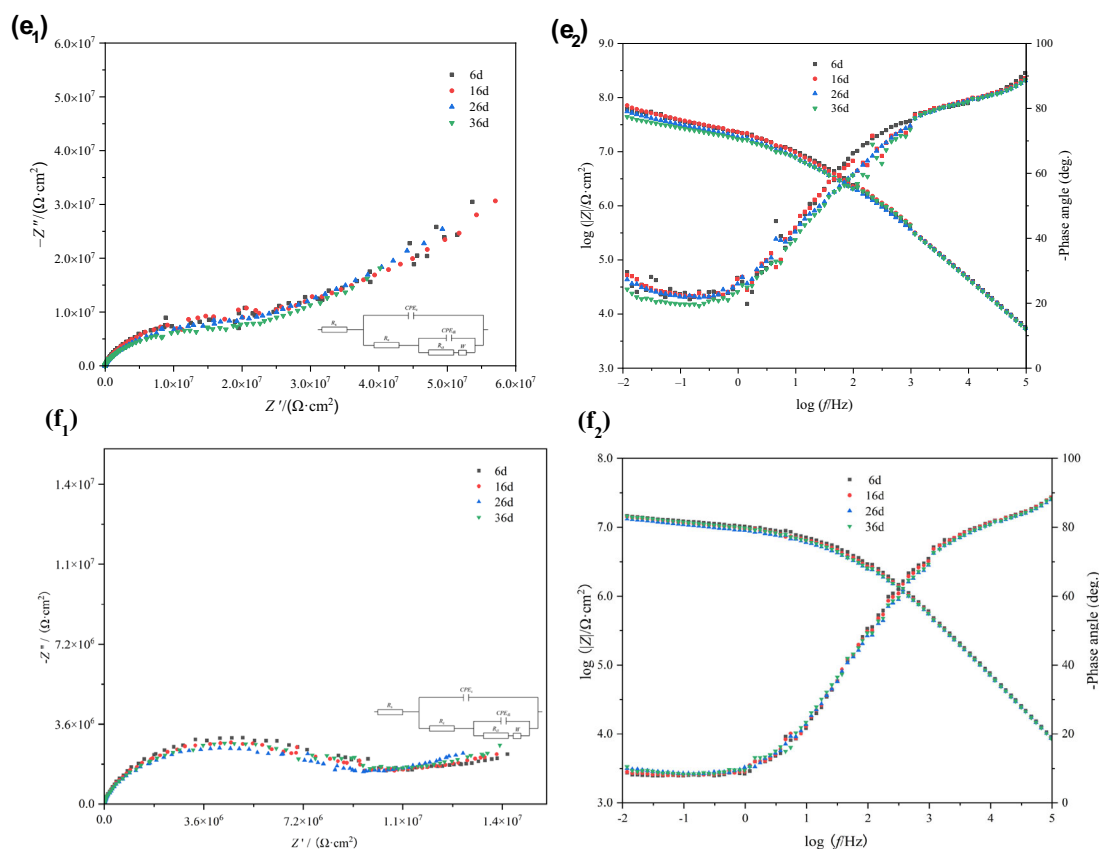


Fig. 5: continued

Table 1: $|Z|_{0.01 \text{ Hz}}$ ($\Omega\text{-cm}^2$) and R_{ct} (36 d) ($\Omega\text{-cm}^2$) of specimens after being immersed in 3.5 wt% NaCl solution for different times

Specimens	Time				
	6 d	16 d	26 d	36 d	R_{ct} (36 d)
EP	8.60×10^5	8.19×10^4	4.96×10^4	1.34×10^4	1.16×10^4
EP/CNTs ₂	5.39×10^6	8.43×10^5	5.44×10^4	3.90×10^3	5.07×10^3
EP/PCNTs ₂	8.84×10^6	3.12×10^6	1.35×10^5	8.16×10^3	1.03×10^4
EP/PCNTs ₄	6.45×10^6	7.96×10^6	5.64×10^6	4.76×10^6	3.94×10^5
EP/PCNTs ₆	6.18×10^7	7.16×10^7	5.55×10^7	4.41×10^7	2.22×10^7
EP/PCNTs ₈	1.48×10^7	1.44×10^7	1.32×10^7	1.45×10^7	1.10×10^7

Characterization of composite epoxy coatings on NdFeB

Figure 4 displays the cross-sectional morphologies of composite epoxy coatings on NdFeB substrate obtained under different conditions. As demonstrated in Figs. 4a1 to 4f1, the thickness of the composite coating increases continuously with the filling amount of PCNTs. Additionally, the thickness change of the specimens is nonlinear with the filling amount of PCNTs. Increasing the PCNTs loading from 2 g/L to 4 g/L results in a minimal increase in coating thickness, as shown in Figs. 4a1 to 4d1, from 16 μm to 16.5 μm and 17 μm, respectively. However, increasing the loading from 4 g/L to 6 g/L results in a much greater growth of the coating thickness, as shown in Figs. 4d1 to 4f1, from 17 μm to 20 μm and 24 μm, respectively.

Electrophoretic deposition is a process where cationic epoxy resin particles migrate to the cathode and deposit on the surface of the substrate under the action of external direct current. When PCNT hybrids are added to the epoxy suspension, some of the hybrids are deposited on the substrate surface along with the epoxy resin particles. As the concentration of PCNTs in the electrophoretic suspension increases, more PCNTs are deposited in the coating, resulting in an increase in coating thickness. Additionally, coating thickness is affected by the compactness of the coating. The aggregation of PCNTs causes a loose structure, which increases the coating thickness under the same electrophoretic deposition parameters. A low loading of PCNTs only increases the coating thickness due to the filling effect, where the thickness increment should be linear to the loading. On the other hand, a high loading of PCNTs increases the coating thickness due to the composite effects of PCNTs filling and density decrease.

The surface morphologies of various specimens can reveal the density changes of composite epoxy coatings, as demonstrated in Figs. 4a2–4f2. Figure 4a2 illustrates the surface morphology of pure EP coatings on NdFeB magnets, which displays numerous micropores that are clearly visible due to the rapid volatilization of water during solidification. Incorporating

2 g/L CNTs into the coating results in a more irregular cross section and poor dispersion of CNTs in the polymer matrix, leading to significant agglomeration and numerous defects (Fig. 4b2). Furthermore, the interface between CNTs and epoxy resin is clearly visible, indicating poor compatibility between CNTs and the epoxy matrix. At the same filling amount (Fig. 4c2), many pores are still visible in the coating for EP/PCNTs₂ specimens. However, the combination between CNTs and resin has improved significantly. As the concentration of PCNTs increases to 4 g/L (Fig. 4d2), the number of pores decreases significantly. In EP/PCNTs₆ (Fig. 4e2) and EP/PCNTs₈ (Fig. 4f2) systems, there are no visible pores, indicating the excellent filling effects of PCNTs in the coating. However, the surface flatness of EP/PCNTs₈ is reduced compared to that of EP/PCNTs₄ and EP/PCNTs₆. This reduction may be due to the aggregation of PCNTs at high loading. In other words, the filling effect of PCNTs is beneficial for eliminating pores and increasing coating thickness. However, PCNTs' aggregation with high loading may decrease the compactness of coatings, resulting in an additional increase in coating thickness.

Anticorrosion performance of composite epoxy coatings on NdFeB

Electrochemical impedance spectroscopy (EIS) measurements were conducted to evaluate the anticorrosion performance of composite epoxy coatings on NdFeB magnets. The measurements were carried out in an electrolyte containing 3.5 wt% NaCl for varying durations. The Nyquist and Bode plots obtained are presented in Fig. 5. The electrical equivalent circuits are shown as inset in the Nyquist patterns, in which the parameters of R_s , R_c , CPE_c , CPE_{dl} , and R_{ct} in the electrical equivalent circuits correspond to solution resistance, coating resistance and coating capacitance, double-layer capacitance and a charge transfer resistance, respectively. The Warburg element (W) indicates the diffusion process of the coating.

Figures 5a1–5c1 shows that all three specimens, EP, EP/CNTs₂, and EP/PCNTs₂, exhibit two arcs at the initial test stage. This demonstrates that the corrosive medium penetrates the coating and reaches the coating/magnet interface. However, it is important to note that over a period of 26 days, the high-frequency capacitive arc radius of EP/CNTs₂ and EP/PCNTs₂ is greater than that of EP specimens, indicating that the addition of CNTs and PCNTs improves the impedance of the specimens, which in turn enhances the corrosion resistance of the epoxy coatings. EP/PCNTs₄, EP/PCNTs₆, and EP/PCNTs₈ specimens exhibit distinct Nyquist plots (Figs. 5d1–5f1) with a high frequency capacitive arc and a slash, indicating the diffusion-controlled corrosion reaction. PCNTs have contributed to the electron exchange behavior of corrosion as an electrochemically active substance.^{56,57} The test extension maintains the arc radiuses of specimens at a high level and the attenuation of the radiuses at a low level, demonstrating excellent corrosion resistance and stability.

The low-frequency impedance modulus ($|Z|_{0.01 \text{ Hz}}$) observed in the Bode plot indicates the coating's protective capacity, with higher $|Z|_{0.01 \text{ Hz}}$ representing better anticorrosion performance.⁵⁸ The Bode plots for

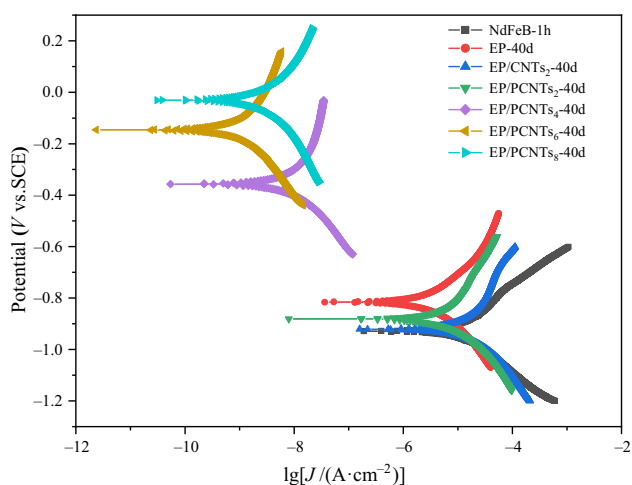


Fig. 6: Potentiodynamic polarization curves of different specimens after being immersed in 3.5 wt% NaCl for 40 days

the prepared specimens are shown in Figs. 5a1–5f1, and Table 1 provides the extracted $|Z|_{0.01 \text{ Hz}}$ values from the plots. During the initial testing period, the $|Z|_{0.01 \text{ Hz}}$ of the EP specimens is as low as $8.60 \times 10^5 \Omega\text{-cm}^2$, indicating poor corrosion resistance. As the test continued, the $|Z|_{0.01 \text{ Hz}}$ value decreases by an order of magnitude to $1.34 \times 10^4 \Omega\text{-cm}^2$ after 36 days of soaking. The coating of EP specimens contains numerous pores and defects, resulting in poor anticorrosion performance. The addition of 2 g/L CNTs and PCNTs to the coating results in an increase in $|Z|_{0.01 \text{ Hz}}$ of EP/CNTs₂ and EP/PCNTs₂ specimens to 5.39×10^6 and $8.84 \times 10^6 \Omega\text{-cm}^2$, respectively. This demonstrates that the anticorrosion performance of the specimens is better than that of EP in the short term. However, after 26 days, $|Z|_{0.01 \text{ Hz}}$ of EP/CNTs₂ decreases to the same order of magnitude as that of EP, while $|Z|_{0.01 \text{ Hz}}$ of EP/PCNTs₂ remains higher than that of EP. It is important to note that the $|Z|_{0.01 \text{ Hz}}$ of EP/CNTs₂ and EP/PCNTs₂ specimens decrease to 3.90×10^3 and $8.16 \times 10^3 \Omega\text{-cm}^2$, respectively, after being immersed for 36 days, which is lower than that of EP, indicating that the composite specimens have poorer anticorrosion performance than EP over a longer period of time. The decrease in $|Z|_{0.01 \text{ Hz}}$ for EP/PCNTs₄, EP/PCNTs₆ and EP/PCNTs₈ specimens with prolonged soaking time may be attributed to microgalvanic corrosion resulting from the disordered connection of CNTs/NdFeB or PCNTs/NdFeB substrate after the corrosion medium reaches the coating/magnet interface,⁵⁹ which leads to more serious corrosion. For EP/PCNTs₄, EP/PCNTs₆, and EP/PCNTs₈ specimens, their $|Z|_{0.01 \text{ Hz}}$ decreases with prolonged soaking time but remains at a high level of approximately $10^6 \Omega\text{-cm}^2$, $10^7 \Omega\text{-cm}^2$, and $10^7 \Omega\text{-cm}^2$ within 36 days, respectively. After being immersed for 36 days, the R_{ct} value of EP/PCNTs₆ is still greater than that of other specimens, and R_{ct} of different specimens shows the same tendency as $|Z|_{0.01 \text{ Hz}}$. To summarize, the addition of appropriate concentrations of PCNTs can significantly improve the corrosion resistance of specimens, which is particularly true when the concentration is 4, 6, or 8 g/L.

It is worth noting that EP/PCNTs₈ exhibit slightly worse $|Z|_{0.01 \text{ Hz}}$ than that of EP/PCNTs₆, despite the former having a higher coating thickness (as shown in Figs. 4e and 5f). This can be attributed to the decrease

Table 2: Electrochemical polarization parameters of different specimens

	$J_{\text{corr}}/(\text{A}\cdot\text{cm}^{-2})$	E_{corr}/V	$-\beta_c(V/\text{dec})$	$\beta_a(V/\text{dec})$	η (%)
NdFeB-1 h	2.302×10^{-5}	- 0.929	0.162	0.197	
EP-40d	4.436×10^{-6}	- 0.816	0.173	0.166	80.23
EP/CNTs ₂ -40d	1.602×10^{-5}	- 0.921	0.166	0.259	30.41
EP/PCNTs ₂ -40d	8.107×10^{-6}	- 0.881	0.164	0.262	64.78
EP/PCNTs ₄ -40d	9.404×10^{-9}	- 0.357	0.171	0.254	95.91
EP/PCNTs ₆ -40d	9.648×10^{-10}	- 0.146	0.180	0.215	99.58
EP/PCNTs ₈ -40d	3.290×10^{-9}	- 0.031	0.197	0.196	98.57

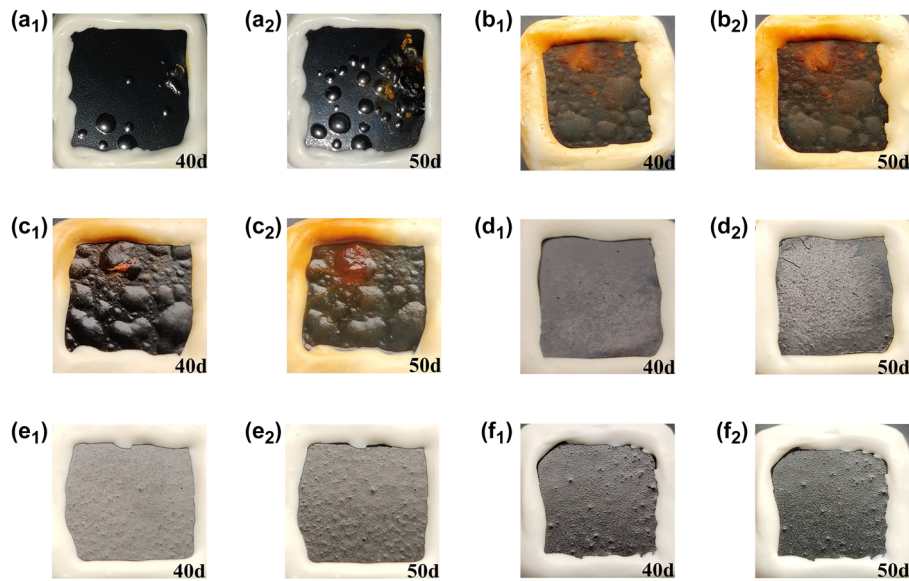


Fig. 7: Optical photographs of EP (a), EP/CNTs₂ (b), EP/PCNTs₂ (c), EP/PCNTs₄ (d), EP/PCNTs₆ (e) and EP/PCNTs₈ (f) after being immersed in 3.5 wt% NaCl solution for 40 d and 50 d

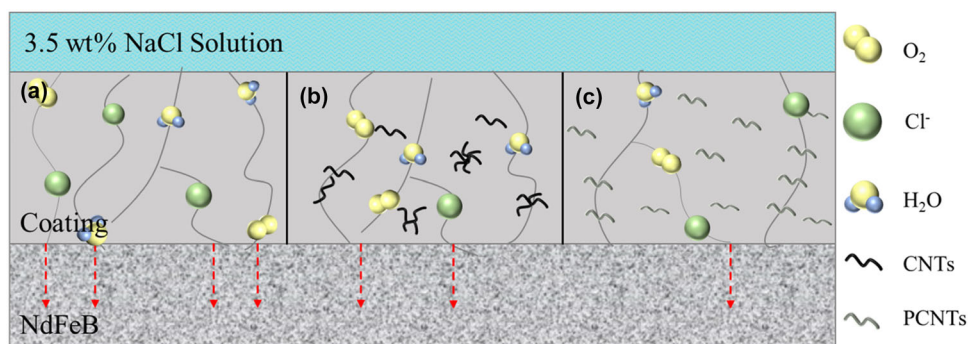


Fig. 8: Corrosion protection mechanism of EP (a), EP/CNTs (b), and EP/PCNTs (c) specimens

in compactness of EP/PCNTs₈ due to the aggregation of PCNTs at high loading.

Figure 6 displays the potentiodynamic polarization curves of various specimens after immersion in a 3.5 wt% NaCl solution for 40 days, and Table 2 lists the corresponding polarization parameters. To provide a comparison, the polarization curve of NdFeB magnets immersed for 1 h is also included. For uncoated NdFeB, the values of E_{corr} and J_{corr} are -0.929 V and $2.302 \times 10^{-5} \text{ A}\cdot\text{cm}^{-2}$, respectively, indicating poor intrinsic corrosion resistance. After being soaked for 40 days, epoxy resin-coated NdFeB magnets exhibit improved anticorrosion performance with a lower J_{corr} and a positive shift of E_{corr} compared to uncoated NdFeB. The addition of 2 g/L CNTs into the coating does not improve the corrosion resistance and even results in a negative effect in a long-term corrosion process. The polarization result of EP/CNTs₂ is similar to that of uncoated NdFeB with an E_{corr} of -0.921 V and a J_{corr} of $1.602 \times 10^{-5} \text{ A}\cdot\text{cm}^{-2}$. When

the same concentration of PCNT hybrids is added, EP/PCNT₂ specimens exhibit an E_{corr} of -0.881 V and a J_{corr} of $8.107 \times 10^{-6} \text{ A}\cdot\text{cm}^{-2}$, respectively. This is much better than that of EP/CNT₂ but worse than that of EP specimens. In summary, the introduction of 2 g/L CNTs or PCNTs has no positive effect and may even have a negative effect on the long-term corrosion resistance of specimens. This finding is consistent with the change tendency of $|Z|_{0.01 \text{ Hz}}$ data.

As the concentration of PCNTs increases, the corrosion tendency of EP/PCNTs₄, EP/PCNTs₆, and EP/PCNTs₈ specimens gradually decreases with E_{corr} positively shifting to -0.357 , -0.146 , and -0.031 V, respectively. And their J_{corr} decreases to 9.404×10^{-9} , 9.648×10^{-10} and $3.290 \times 10^{-9} \text{ A}\cdot\text{cm}^{-2}$, which shows an extremely low corrosion rate even after soaking for 40 days. Based on the results of EIS and polarization curves, it can be concluded that the addition of PCNTs hybrids with appropriate content to the epoxy resin coating can effectively enhance the

corrosion resistance of the specimens, such as EP/PCNTs₄, EP/PCNTs₆, and EP/PCNTs₈.

To investigate changes to specimen surfaces over time, a static immersion corrosion test was conducted by immersing them in a 3.5 wt% NaCl solution. Figures 7a1 and 7a2 shows that after 40 days of soaking, the EP has bulged and corroded. Additionally, with a soaking period of 50 days, the corrosion area of the EP specimens continues to enlarge. The addition of 2 g/L CNTs into the coating (Figs. 7b1 and 7b2) exacerbates the surface state of the specimens, resulting in more severe surface bulging and corrosion. Similarly, at the same dropping amount (Figs. 7c1 and 7c2), the surface of EP/PCNTs₂ exhibits bulging and corrosion in a large area. The cross-sectional morphologies of coatings in Fig. 4 reveal numerous micropores in all three specimens. The shielding performance of the EP/CNTs₂ coating is poor due to inadequate dispersion and compatibility of CNTs within the coating. Although the dispersion and compatibility of PCNTs with the coating have improved, they are unable to effectively fill the coating's pores. As a result, all three specimens exhibit poor corrosion resistance, leading to noticeable corrosion. A continuous increase in PCNTs' concentration to 4 g/L (Figs. 7d1 and 7d2), 6 g/L (Figs. 7e1 and 7e2), and 8 g/L (Figs. 7f1 and 7f2) results in effective pore filling and improves structural integrity of the coatings. As a result, all three specimens exhibit excellent corrosion resistance with no visible corrosion on the surface even after 50 days of immersion. These results are consistent with the findings of the electrochemical tests.

Mechanism of corrosion protection

Based on the previously presented data, the introduction of suitable PCNT hybrids into the epoxy coatings results in a significant improvement in the specimens' corrosion resistance. The potential protective mechanisms are discussed below. In EP systems (as shown in Fig. 8a), defects resulting from water volatilization during the solidification process can create a diffusion channel for corrosive species to penetrate the interface between the coating and magnet. This is detrimental to the long-term service of specimens in corrosive environments. For EP/CNTs specimens (as shown in Fig. 8b), the addition of CNTs to the coating does not effectively shield the corrosive medium. In fact, it can even decrease the anticorrosion capability of the specimens due to the poor dispersion of CNTs in the epoxy matrix. In addition, modifying CNTs with PEDOT (as shown in Fig. 8c) enhances the compatibility between CNTs and epoxy resin. Furthermore, PSS enables the PCNTs hybrids to achieve a desirable dispersion in the resin, improving the integrity and compactness of the coating and enhancing its resistance to corrosive medium. As a result, the EP/PCNTs specimens exhibit significantly enhanced corrosion resistance.

The concentration of PCNTs hybrids has an impact on both the coating structure and the final corrosion resistance. Low loading, such as EP/PCNTs₂, can even decrease the long-term corrosion resistance due to the microgalvanic corrosion that forms as a result of the disordered connection between the PCNTs and NdFeB substrate after the corrosion medium reaches the coating/magnet interface. High loadings, on the other hand, can produce a good filling effect, but can also lead to reduced densification due to the aggregation of the complex. The specimens' corrosion resistance reaches its optimal value at a loading of 6 g/L. However, when the loading of PCNTs increases to 8 g/L, the corrosion resistance slightly decreases.

Conclusions

PCNT hybrids were prepared by modifying CNTs with PSS and PEDOT. These hybrids were then used as fillers in the preparation of EP/PCNT composite coatings on NdFeB magnets using the cathodic electrophoretic deposition technique. The coating shows no visible pores as the concentration of PCNTs increases, indicating excellent filling effects of PCNTs. However, a high loading of PCNTs results in their aggregation and low compactness, which is reflected in a rougher surface and higher thickness. The $|Z|_{0.01 \text{ Hz}}$ of the optimized EP/PCNTs₆ increases from 1.34×10^4 to $4.41 \times 10^7 \Omega \cdot \text{cm}^2$, while J_{corr} decreases from $4.436 \times 10^{-6} \text{ A} \cdot \text{cm}^{-2}$ to $5.281 \times 10^{-11} \text{ A} \cdot \text{cm}^{-2}$ when compared to pristine EP specimens. The enhanced anticorrosion performance of EP/PCNTs specimens is attributed to the suitable compatibility and dispersity of PCNTs within the epoxy coating, which can enhance the coating's integrity and compactness, thereby delaying damage and failure of the specimens. However, increasing the PCNTs content to 8 g/L deteriorates the corrosion resistance due to the aggregation of PCNTs.

Acknowledgments This work was financially supported by National Key R&D Program of China (Grant No. 2022YFB3504800) and Fundamental Research Funds for the Central Universities (PA2022GDGP0029, PA2023GDGP0042).

References

1. Coey, JMD, "Perspective and Prospects for Rare Earth Permanent Magnets." *Engineering*, **6** (2) 119–131 (2020)
2. Mao, S, Yang, H, Li, J, et al. "The Properties of Aluminium Coating on Sintered NdFeB by DC Magnetron Sputtering." *Vacuum*, **85** (7) 772–775 (2011)
3. Cao, JL, He, JY, Yu, ZG, et al. "Alloying Pr-Tb-Cu Diffusion Source with Ni for Enhancing Both Coercivity and Corrosion Resistance of Nd-Fe-B Magnets." *J. Alloys Compd.*, **911** 165049 (2022)

4. Cao, YJ, Liu, YH, Zhang, PJ, et al. “Corrosion Resistance and Mechanical Properties of (Ho, Nd)FeB Magnets.” *J. Rare Earths*, **39** (11) 1409–1414 (2021)
5. Wu, YP, Zhu, MG, Sun, QS, et al. “Superior Corrosion Resistance and Corrosion Mechanism of Dual-Main-Phase (Ce₁₅Nd₈₅)₃₀Fe_{bal}B₁M Magnets in Different Solutions.” *J. Rare Earths*, **41** (1) 122–129 (2023)
6. Wang, ZX, Pei, K, Zhang, JJ, et al. “Correlation Between the Microstructure and Magnetic Configuration in Coarse-Grain Inhibited Hot-Deformed Nd-Fe-B Magnets.” *Acta Mater.*, **167** 103–111 (2019)
7. Liang, L, Ma, T, Wu, C, et al. “Coercivity Enhancement of Dy-Free Nd-Fe-B Sintered Magnets by Intergranular Adding Ho_{63.4}Fe_{36.6} Alloy.” *J. Magn. Magn. Mater.*, **397** 139–44 (2016)
8. He, J, Liao, X, Lan, X, et al. “Annealed Al-Cr Coating: A Hard Anti-corrosion Coating with Grain Boundary Modification Effect for Nd-Fe-B Magnets.” *J. Alloys Compd.*, **870** 159229 (2021)
9. Ye, CT, Jia, LN, Xu, GX, et al. “Microstructure and Initial Corrosion Behavior of Double-Layer Zn-Al-Mg Coatings Produced by PVD.” *Surf. Coat. Technol.*, **366** 214–226 (2019)
10. Zhang, PJ, Zhu, MG, Li, W, et al. “Study on Preparation and Properties of CeO₂/Epoxy Resin Composite Coating on Sintered NdFeB Magnet.” *J. Rare Earths*, **36** (5) 544–551 (2018)
11. Xu, JL, Xiao, QF, Mei, DD, et al. “Preparation and Characterization of Amorphous SiO₂ Coatings Deposited by Micro-Arc Oxidation on Sintered NdFeB Permanent Magnets.” *J. Magn. Magn. Mater.*, **426** 361–368 (2017)
12. Xu, JL, Xiao, QF, Mei, DD, et al. “Microstructure, Corrosion Resistance and Formation Mechanism of Alumina Micro-Arc Oxidation Coatings on Sintered NdFeB Permanent Magnets.” *Surf. Coat. Technol.*, **309** 621–627 (2017)
13. Duan, LS, Chen, J, Zhang, PJ, et al. “Organic-Inorganic Composite Passivation and Corrosion Resistance of Zinc Coated NdFeB Magnets.” *J. Alloys Compd.*, **936** 168292 (2023)
14. Ding, XF, Wu, YJ, Yang, LJ, et al. “The Properties of Chromium Oxide Coatings on NdFeB Magnets by Magnetron Sputtering with Ion Beam Assisted Deposition.” *Vacuum*, **131** 127–134 (2016)
15. Hu, JM, Liu, XL, Zhang, JQ, et al. “Corrosion Protection of Nd-Fe-B Magnets by Silanization.” *Prog. Org. Coat.*, **55** (4) 388–392 (2006)
16. Xu, JL, Huang, ZX, Luo, JM, et al. “Effect of Titania Particles on the Microstructure and Properties of the Epoxy Resin Coatings on Sintered NdFeB Permanent Magnets.” *J. Magn. Magn. Mater.*, **355** 31–36 (2014)
17. Jin, FL, Li, X, Park, SJ, “Synthesis and Application of Epoxy Resins: A Review.” *J. Ind. Eng. Chem.*, **29** 1–11 (2015)
18. Li, S, Du, F, Lin, Y, et al. “Excellent Anti-Corrosion Performance of Epoxy Composite Coatings Filled with Novel N-doped Carbon Nanodots.” *Eur. Polym. J.*, **163** 110957 (2022)
19. Zhao, Z, Zhou, M, Zhao, W, et al. “Anti-corrosion Epoxy/Modified Graphene Oxide/Glass Fiber Composite Coating with Dual Physical Barrier Network.” *Prog. Org. Coat.*, **167** 106823 (2022)
20. Keshmiri, N, Najmi, P, Ramezanzadeh, M, et al. “Designing an Eco-Friendly Lanthanide-Based Metal Organic Framework (MOF) Assembled Graphene-Oxide with Superior Active Anti-Corrosion Performance in Epoxy Composite.” *J. Clean. Prod.*, **319** 128732 (2021)
21. Lu, F, Liu, C, Chen, Z, et al. “Polypyrrole-Functionalized Boron Nitride Nanosheets for High-Performance Anti-Corrosion Composite Coating.” *Surf. Coat. Technol.*, **420** 127273 (2021)
22. Wan, S, Chen, H, Cai, G, et al. “Functionalization of h-BN by the Exfoliation and Modification of Carbon Dots for Enhancing Corrosion Resistance of Waterborne Epoxy Coating.” *Prog. Org. Coat.*, **165** 106757 (2022)
23. Rostami, M, Rasouli, S, Ramezanzadeh, B, et al. “Electrochemical Investigation of the Properties of Co Doped ZnO Nanoparticle as a Corrosion Inhibitive Pigment for Modifying Corrosion Resistance of the Epoxy Coating.” *Corros. Sci.*, **88** 387–399 (2014)
24. Hu, C, Li, Y, Kong, Y, et al. “Preparation of Poly(o-toluidine)/Nano ZnO/Epoxy Composite Coating and Evaluation of Its Corrosion Resistance Properties.” *Synth. Metals*, **214** 62–70 (2016)
25. Qian, Y, Zheng, W, Chen, WG, et al. “Enhanced Functional Properties of CeO₂ Modified Graphene/Epoxy Nanocomposite Coating Through Interface Engineering.” *Surf. Coat. Technol.*, **409** 126819 (2021)
26. Zare, EN, Lakouraj, MM, Moosavi, E, “Poly(3-aminobenzoic acid)/MWCNTs Hybrid Conducting Nanocomposite: Preparation, Characterization, and Application as a Coating for Copper Corrosion Protection.” *Compos. Interfaces*, **23** (7) 571–583 (2016)
27. Najmi, P, Keshmiri, N, Ramezanzadeh, M, et al. “Synthesis and Application of Zn-doped Polyaniline Modified Multi-walled Carbon Nanotubes as Stimuli-Responsive Nanocarrier in the Epoxy Matrix for Achieving Excellent Barrier-Self-healing Corrosion Protection Potency.” *Chem. Eng. J.*, **412** 128637 (2021)
28. Situ, Y, Ji, W, Liu, C, et al. “Synergistic Effect of Homogeneously Dispersed PANI-TiN Nanocomposites Towards Long-Term Anticorrosive Performance of Epoxy Coatings.” *Prog. Org. Coat.*, **130** 158–167 (2019)
29. Chen, C, Qiu, S, Cui, M, et al. “Achieving High Performance Corrosion and Wear Resistant Epoxy Coatings via Incorporation of Noncovalent Functionalized Graphene.” *Carbon*, **114** 356–366 (2017)
30. Nayak, SR, Mohana, KNS, Hegde, MB, et al. “Functionalized Multi-Walled Carbon Nanotube/Polyindole Incorporated Epoxy: An Effective Anti-Corrosion Coating Material for Mild Steel.” *J. Alloys Compd.*, **856** 158057 (2021)
31. Cui, M, Ren, S, Qiu, S, et al. “Non-covalent Functionalized Multi-wall Carbon Nanotubes Filled Epoxy Composites: Effect on Corrosion Protection and Tribological Performance.” *Surf. Coat. Technol.*, **340** 74–85 (2018)
32. Wen, Y, Xu, J, “Scientific Importance of Water-Processable PEDOT-PSS and Preparation, Challenge and New Application in Sensors of Its Film Electrode: A Review.” *J. Polym. Sci. Part A: Polym. Chem.*, **55** (7) 1121–1150 (2017)
33. Zhang, SJ, Li, M, Zhai, LJ, “Preparation and Corrosion Inhibition of Single and Biphasic Composite Coating Based on PEDOT in 0.1M NaOH.” *Int. J. Electrochem. Sci.*, **14** (5) 4828–37 (2019)
34. Zhang, M, Gao, B, Liu, J, et al. “The Stability of Poly(3, 4-ethylenedioxythiophene) Based on Electrochemical Polymerization and Photoelectro-Corrosion Conditions.” *Polym. Degrad. Stab.*, **198** 109881 (2022)
35. Hou, J, Zhu, G, Xu, JK, et al. “Epoxy Resin Modified with PEDOT/PSS and Corrosion Protection of Steel.” *Mater. Sci. Technol.*, **560–561** 947–951 (2012)
36. Su, Y, “PEDOT: PSS-exfoliated Graphene to Improve the Corrosion Resistance of Waterborne Epoxy Coating.” *Int. J. Electrochem. Sci.*, **14** 4595–610 (2019)
37. Hou, J, Zhu, G, Xu, J, et al. “Anticorrosion Performance of Epoxy Coatings Containing Small Amount of Inherently

- Conducting PEDOT/PSS on Hull Steel in Seawater.” *J. Mater. Sci. Technol.*, **29** (7) 678–84 (2013)
38. Abdullah, WRW, Ibrahim, NF, Arifin, SNSM, et al. “Corrosion Inhibition and Antifouling Performance of Epoxy Coating Functionalized with PEDOT: PSS-Cerium Doped Zinc Oxide Hybrid Composites.” *IOP Conf. Ser.: Mater. Sci. Eng.*, **864** (1) 012003 (2020)
 39. Xiong, S, Zhang, J, Wang, X, et al. “Electrochemical Synthesis of Covalently Bonded Poly(3,4-dioxyethylthiophene)–Carbon Nanotubes Composite with Enhanced Electrochromic Properties.” *J. Electron. Mater.*, **50** (4) 2389–2399 (2021)
 40. Türkmen, TA, Taşaltın, N, Taşaltın, C, et al. “PEDOT: PSS/ β_{12} Borophene Nanocomposites as an Inorganic–Organic Hybrid Electrode for High Performance Supercapacitors.” *Inorgan. Chem. Commun.*, **139** 109329 (2022)
 41. Mitraga, E, Jafari, MJ, Vagin, M, Liu, X, Fahlman, M, Ederth, T, Berggren, M, Jonsson, MP, Crispin, X, “Oxygen-Induced Doping on Reduced PEDOT.” *J. Mater. Chem. A*, **5** 4404–4412 (2017)
 42. Gülercan, D, Gergin, İ, Sarac, AS, “Preparation and Electrochemical Performances of Graphene Oxide/PEDOT and Reduced Graphene Oxide/PEDOT Nanofibers and Nanocomposites.” *Fibers Polymers*, **19** (10) 2178–2187 (2018)
 43. Zhang, J, Zhao, XS, “Conducting Polymers Directly Coated on Reduced Graphene Oxide Sheets as High-Performance Supercapacitor Electrodes.” *J. Phys. Chem. C*, **116** (9) 5420–5426 (2012)
 44. Zhang, S, Ren, J, Zhang, Y, et al. “PEDOT Hollow Nanospheres for Integrated Bifunctional Electrochromic Supercapacitors.” *Organ. Electron.*, **77** 105497 (2020)
 45. Xiong, S, Zhang, J, Wu, B, et al. “Electrochemical Preparation of Covalently Bonded PEDOT–Graphene Oxide Composite Electrochromic Materials Using Thiophene-2-methylaniline as Bridging Group.” *ChemistrySelect*, **5** (39) 12206–12212 (2020)
 46. Lu, F, Chen, Y, Mao, X, et al. “PEDOT: PSS/PEDOT Composite Film for High Performance Electrochemical Electrode.” *AIP Conf. Proc.*, **1794** (1) 020015 (2017)
 47. Zhang, X, Huang, Y, Huang, X, et al. “Facile Synthesis and Characterisation of SiO_2 @PSS/Ag-PPy Using SiO_2 @PSS as Template.” *Micro Nano Lett.*, **10** (3) 153–156 (2015)
 48. García-Barberá, A, Culebras, M, Roig-Sánchez, S, et al. “Three Dimensional PEDOT Nanowires Network.” *Synth. Metals*, **220** 208–212 (2016)
 49. Illakkiya, JT, Rajalakshmi, PU, Oommen, R, “Synthesis and Characterization of Transparent Conducting SWCNT/PEDOT: PSS Composite Films by Spin Coating Technique.” *Optik*, **157** 435–40 (2018)
 50. Madhan Kumar, A, Mizanur Rahman, M, Gasem, ZM, “A Promising Nanocomposite from CNTs and Nano-ceria: Nanostructured Fillers in Polyurethane Coatings for Surface Protection.” *RSC Adv.*, **5** (78) 63537–63544 (2015)
 51. Zheng, X, Xu, J, Yan, K, et al. “Space-Confined Growth of MoS_2 Nanosheets within Graphite: The Layered Hybrid of MoS_2 and Graphene as an Active Catalyst for Hydrogen Evolution Reaction.” *Chem. Mater.*, **26** (7) 2344–2353 (2014)
 52. Zhu, L, Feng, C, Cao, Y, “Corrosion Behavior of Epoxy Composite Coatings Reinforced with Reduced Graphene Oxide Nanosheets in the High Salinity Environments.” *Appl. Surf. Sci.*, **493** 889–896 (2019)
 53. Ge, Y, Jamal, R, Zhang, R, et al. “Electrochemical Synthesis of Multilayered PEDOT/PEDOT-SH/Au Nanocomposites for Electrochemical Sensing of Nitrite.” *Mikrochim. Acta*, **187** (4) 248 (2020)
 54. Vitoratos, E, Sakkopoulos, S, Dalas, E, et al. “Thermal Degradation Mechanisms of PEDOT:PSS.” *Organ. Electron.*, **10** (1) 61–66 (2009)
 55. Bianchi, M, Carli, S, Di Lauro, M, et al. “Scaling of Capacitance of PEDOT:PSS: Volume vs. Area.” *J. Mater. Chem. C*, **8** (32) 11252–11262 (2020)
 56. Ruhi, G, Bhandari, H, Dhawan, SK, “Designing of Corrosion Resistant Epoxy Coatings Embedded with Polypyrrole/ SiO_2 Composite.” *Prog. Org. Coat.*, **77** (9) 1484–1498 (2014)
 57. Jacobsen, T, West, K, “Diffusion Impedance in Planar, Cylindrical and Spherical Symmetry.” *Electrochim. Acta*, **40** (2) 255–262 (1995)
 58. Wu, Y, Jiang, F, Qiang, Y, et al. “Synthesizing a Novel Fluorinated Reduced Graphene Oxide- CeO_2 Hybrid Nanofiller to Achieve Highly Corrosion Protection for Waterborne Epoxy Coatings.” *Carbon*, **176** 39–51 (2021)
 59. Yazdani, S, Mahboubi, F, Tima, R, et al. “Effect of Carbon Nanotube Concentration on the Corrosion Behavior of Electroless Ni-B-CNT Coating.” *J. Mater. Eng. Perform.*, **28** (6) 3446–3459 (2019)

Publisher’s Note Springer Nature remains neutral with regard to jurisdictional claims in published maps and institutional affiliations.

Springer Nature or its licensor (e.g. a society or other partner) holds exclusive rights to this article under a publishing agreement with the author(s) or other rightsholder(s); author self-archiving of the accepted manuscript version of this article is solely governed by the terms of such publishing agreement and applicable law.